THE JOURNAL OF PHYSICAL CHEMISTRY Letters

Letter

Cite This: J. Phys. Chem. Lett. 2019, 10, 4744−4751

pubs.acs.org/JPCL

Putting the Squeeze on Lead Chromate Nanorods

Hongsheng Yuan,[†] Placida Rodriguez-Hernandez,[‡] Alfonso Muñoz,[‡] and Daniel Errandonea*[,§]

[†]Center for High Pressure Science and Technology Advanced Research (HPSTAR), 1690 Cailun Road, BLDG 6, Pudong, Shanghai 201203, P.R. China

[‡]Departamento Física, Malta Consolider Team and Instituto de Materiales y Nanotecnología, Universidad de La Laguna, 38206 La Laguna, Tenerife, Spain

[§]Departamento de Física Aplicada-ICMUV, Universidad de Valencia, MALTA Consolider Team, Edificio de Investigación, C. Dr. Moliner 50, 46100 Burjassot, Spain

Supporting Information

ABSTRACT: We have studied by means of X-ray diffraction and Raman spectroscopy the high-pressure behavior of $PbCrO_4$ nanorods. We have found that these nanorods follow a distinctive structural sequence that differs from that of bulk $PbCrO_4$. In particular, a phase transition from a monoclinic monazite-type $PbCrO_4$ to a novel monoclinic $AgMnO_4$-type polymorph has been discovered at 8.5 GPa. The crystal structure, Raman-active phonons, and compressibility of this novel high-pressure phase are reported for the first time. The experimental findings are supported by ab initio calculations that provide information not only on structural and vibrational properties of $AgMnO_4$-type $PbCrO_4$ but also on the electronic properties. The discovered phase transition triggers a band gap collapse and a subsequent metallization at 44.2 GPa, which has not been observed in bulk $PbCrO_4$. This suggests that nanoengineering can be a useful strategy to drive metallization under compression.

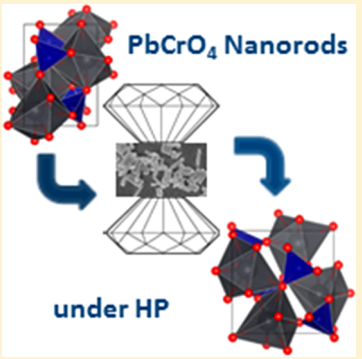

$PbCrO_4$ is a semiconductor with a monoclinic monazite-type structure (space group $P21/n$),[1] which is shown in Figure 1. This material has recently received a great amount of attention from both fundamental and applied research. Its applications are many, going from optoelectronic[2] to photocatalytic water splitting[3,4] and degradation of pollutants under visible-light irradiation.[5,6] For optimizing them, it is necessary to accurately characterize the physical properties of $PbCrO_4$. This information is also relevant for understanding the manufacturing processes of objects of cultural and historical significance; like Kandinsky's reverse paintings on glass.[7] It is also relevant for geophysical studies and for radioactive waste management.[8] As a consequence, several studies have been performed in order to improve the characterization of $PbCrO_4$ at ambient,[9] high-pressure (HP),[10−13] low-temperature,[14] and high-temperature (HT) conditions,[15] as well as to develop green synthesis methods for nanoscale $PbCrO_4$.[16,17] One of the most relevant achievements on the study of $PbCrO_4$ is the discovery of a very rich polymorphism. An orthorhombic Barite-type polymorph (space group *Pnma*) has been reported at HT,[15] and a sequence of phase transitions has been observed under HP.[12,13] These transitions include a transformation to a tetragonal scheelite-type polymorph (space group $I4_1/a$) and a subsequent transformation to an orthorhombic distortion of Barite (space group $P2_12_12_1$). All these studies have been carried out either in natural samples (mineral crocoite) or in bulk materials. The HP properties of $PbCrO_4$ nanomaterials have not been studied yet.

It is known that the investigation of nanomaterials under HP offers new avenues for the study of fundamental phenomena and for the creation of new polymorphs with enhanced properties.[18] Essentially, the volume reduction associated with compression favors the interaction among nanoobjects. This, combined with the relevance of surface atoms in nanomaterials, leads in many nanocompounds to phase transitions that do not exist in their bulk counterpart. In the case, of $PbCrO_4$, this is a reasonable way for the creation of new polymorphs with a modified electronic structure and a band gap energy close to the Shockley−Queisser optimum bandgap (1.34 eV).[19]

In this work we present a combined experimental and theoretical study of $PbCrO_4$ nanorods up to 15 GPa, reporting the existence of a new monoclinic polymorph at pressures higher than 8 GPa, which has an electronic band gap smaller than the ambient-pressure monazite-type polymorph and is predicted to metallize at 44.2 GPa.

In Figure 2a we present a scanning electron microscopy (SEM) image of the synthesized nanorods. It reveals that the as-synthesized submicron crystals were uniform with a rodlike morphology. The results of the dimension analysis of 100 rods are shown in Figure 2b. The average diameter is 330 nm with a standard deviation of 130 nm and a length of 1100 nm with a standard deviation of 120 nm. Energy-dispersive X-ray analysis (EDX) shows that in the synthesized nanorods the molar ratio

Received: July 8, 2019
Accepted: August 5, 2019
Published: August 5, 2019

DOI: 10.1021/acs.jpclett.9b01978
J. Phys. Chem. Lett. 2019, 10, 4744−4751

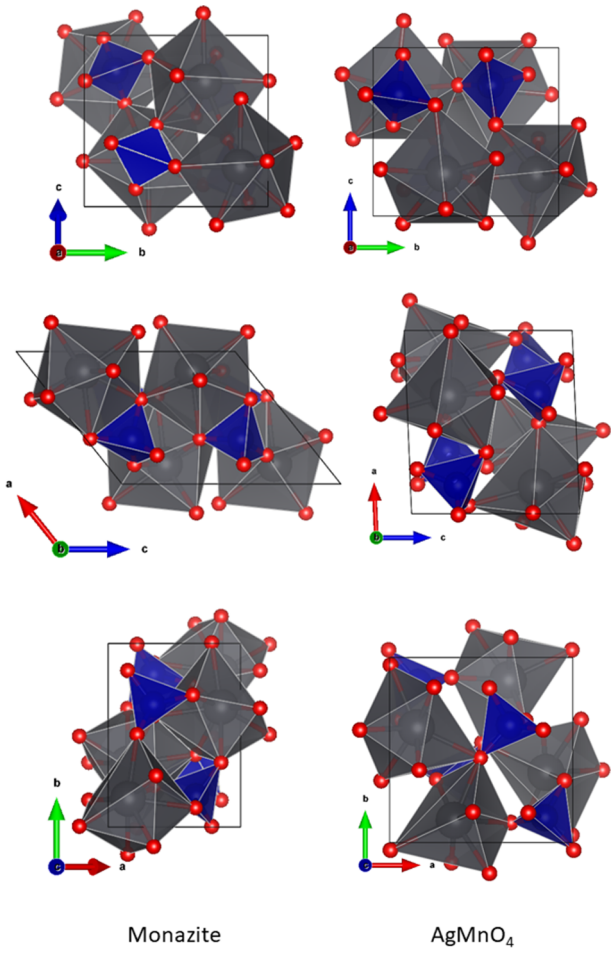

Figure 1. Schematic view of the crystal structure of monazite-type (left) and $AgMnO_4$-type $PbCrO_4$. The coordination polyhedra of Pb and Cr are shown in gray and blue. The red spheres are the oxygen atoms.

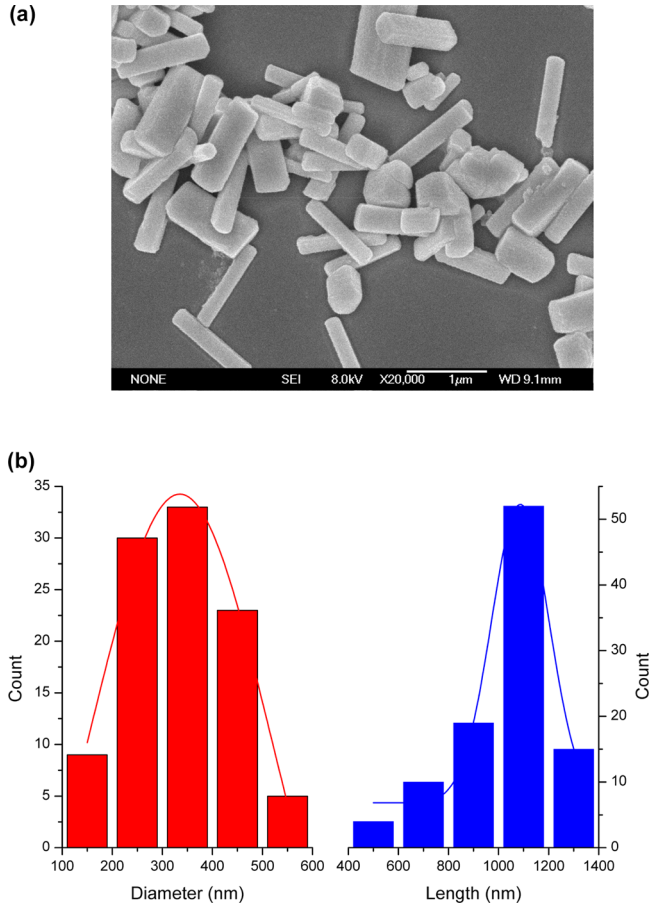

Figure 2. (a) SEM image of $PbCrO_4$ nanorods. (b) Histograms of nanorods dimensions. The lines are the Gaussian fits.

of Pb, Cr, and O is close to 1:1:4 (Pb 16.8 at%, Cr 16.6 at%, and O 66.6 at%), indicating stoichiometric $PbCrO_4$ was successfully prepared. Powder X-ray diffraction (XRD) measurements determined the crystal structure to be monazite-type with unit-cell parameters a = 7.091(4) Å, b = 7.398(4) Å, c = 6.782(3) Å, and β = 102.51(2)°, the unit-cell volume (V = 347.3(6) Å^3) of the nanorods being 1.3% smaller than that of the bulk counterpart.

In Figure 3 we show a selection of HP powder XRD measurements collected under quasi hydrostatic conditions. The XRD patterns measured up to 7 GPa can be undoubtedly assigned to the low-pressure monoclinic monazite structure. This is illustrated by the Rietveld refinement performed at 0.5 GPa where all the peaks can be matched up with the monazite structure with small residuals (R_p = 4.63%, R_{wp} = 6.63%, and χ^2 = 1.98). Up to 7 GPa only a gradual evolution of the XRD patterns was observed with no qualitative changes and peaks moving toward high angles due to the contraction of the crystal structure. At 7.9 GPa we found the appearance of many new peaks (the most evident ones are depicted by asterisks in the figure). The appearance of these peaks is indicative of the onset of a phase transition, which is consistent with our findings from Raman experiments and density-functional theory calculations. Upon further compression we observed the phase coexistence up to approaching 9.4 GPa. At this pressure all the XRD peaks can be assigned to the HP phase. We have identified the crystal structure of the HP phase and it is different from any of the previously reported polymorphs. This means that the structural sequence followed by $PbCrO_4$ nanorods under compression is different from that of its bulk counterpart. As in other oxides,[18,20] probably, in $PbCrO_4$ nanorods, particle-size effects lead to the different phase transition routes compared to the bulk counterpart.

After trying several postmonazite structure reported in the literature,[21−24] we have found that the crystal structure of the HP polymorph can be assigned to a structure isomorphic to $AgMnO_4$. The results of the Rietveld refinement considering this structure are shown in Figure 3. The quality of the refinement is similar to that obtained for the low-pressure phase, supporting the identification of the HP polymorph as the $AgMnO_4$-type. In the figure it can be seen that the residuals are small. In this case the quality refinement parameters are R_p = 4.32%, R_{wp} = 5.63%, and χ^2 = 1.76. The unit-cell parameters are a = 6.788(7) Å, b = 6.954(7) Å, c = 6.255(7) Å, and β 92.80(4)°, which gives V = 294.9(9) Å^3. More information on the crystal structure of $AgMnO_4$-type $PbCrO_4$ is given in Table S1 of the Supporting Information. The HP structure is shown in Figure 1. Notice that it can be described by the same space group as for the low-pressure monazite structure. However, the phase transition implies a very important structural restructuration, with a collapse of the b- and c-axes, an expansion of the a-axis, and a considerable decrease of the monoclinic β angle. The coordination polyhedra are consequently distorted,

DOI: 10.1021/acs.jpclett.9b01978
J. Phys. Chem. Lett. 2019, 10, 4744−4751

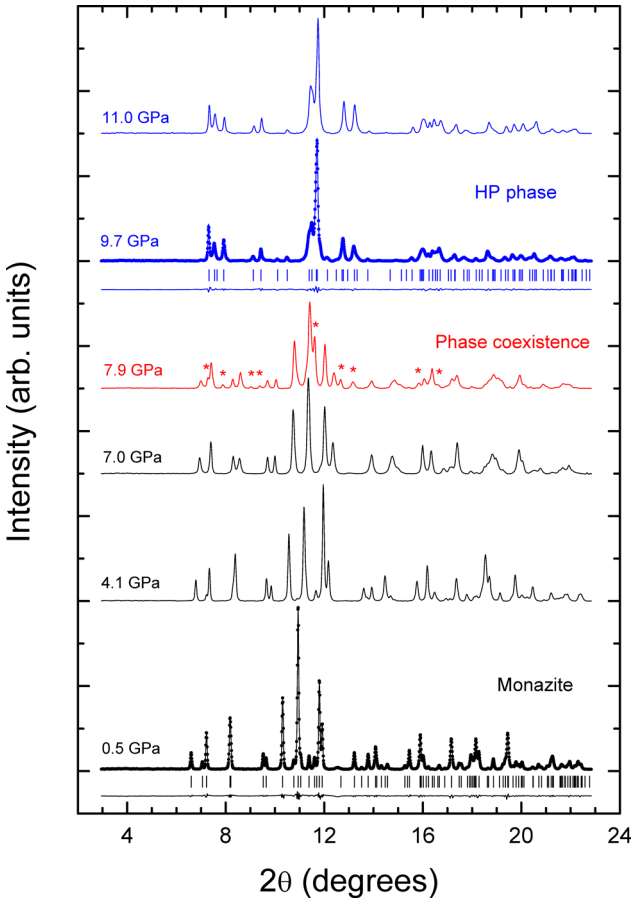

Figure 3. Powder XRD patterns measured for $PbCrO_4$ nanorods. Patterns assigned to the low-pressure monazite phase are shown in black. Patterns of the HP phase are shown in blue. In the pattern measured at 7.9 GPa (shown in red) the coexistence of the two phases is observed. At 0.5 and 9.4 GPa the dots correspond to the experiments. The lines to the refinements and residuals and the ticks to the position of Bragg peaks.

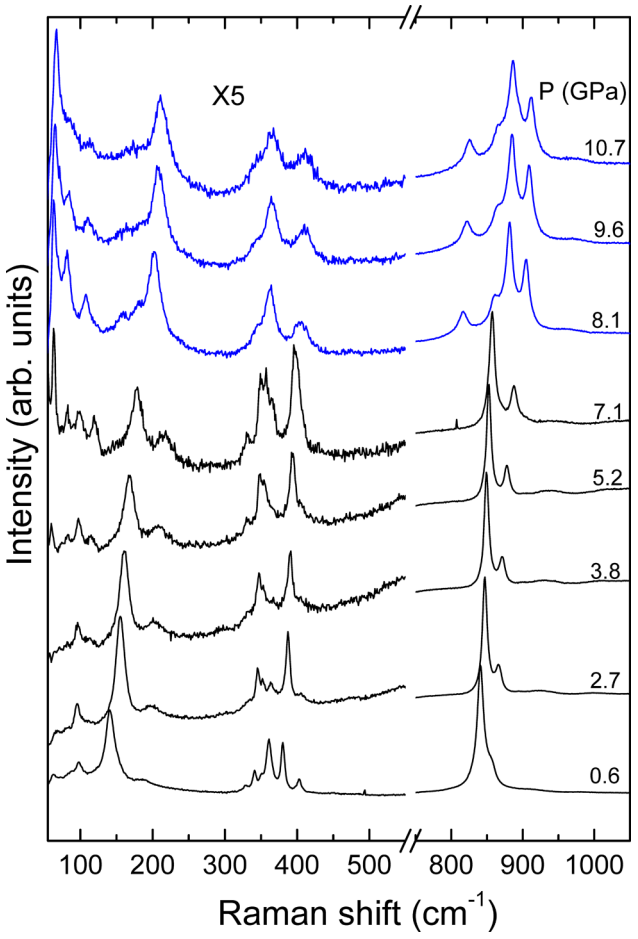

Figure 4. Raman spectra of $PbCrO_4$ nanorods at different pressures (indicated in the figure). The low-frequency region has been magnified five times. We show in black (blue) the spectra from the low(high)-pressure phase.

becoming more irregular than in the low-pressure monazite phase. This has consequences on the electronic and vibrational properties. In addition, the transition involves a volume collapse of the unit-cell volume of 2.5%. The new HP polymorph is a distortion of the Barite structure with few structural similarities with the monazite structure.

In Figure 4 we show a selection of Raman spectra measured at different pressures. The spectra measured from ambient pressure up to 7.1 GPa are very similar to those reported for monazite $PbCrO_4$ in the literature,[10,13] where the pressure evolution of Raman modes of monazite-type $PbCrO_4$ has been already discussed in detail. We will focus here ion changes observed beyond 7.1 GPa. As can been seen in the figure, there is a substantial change in the Raman spectrum from 7.1 to 8.1 GPa. This fact confirms the occurrence of the phase transition detected in XRD experiments. The Raman spectrum of the HP phase is very different from that of the scheelite-type HP polymorph discovered in single-crystal studies on bulk $PbCrO_4$.[13] This phase only has 13 Raman-active modes and three modes above 800 cm^{-1}, while we detect here 20 modes at 8.1 GPa, with four of them for wavenumbers larger than 800 cm^{-1}. However, the Raman spectra measured here at 8.1 GPa and higher pressures also differ from those reported by Bandiello et al. from natural $PbCrO_4$.[10] Therefore, the present Raman experiment support the existence of a new polymorph in $PbCrO_4$ that is different from all the polymorphs found in previous studies on bulk $PbCrO_4$. It has been stablished that the high-frequency Raman modes in $PbCrO_4$ are associated with internal vibrations of the CrO_4 tetrahedron, which do not involve any movement of the Pb cation or the center of mass of CrO_4.[1] Thus, the increase of the number of modes in the high-frequency region of the $AgMnO_4$-type polymorph of $PbCrO_4$ in comparison with the previously known HP scheelite-type polymorph[13] is a consequence of the distortion induced by the phase transition in the CrO_4 polyhedron.

In Figure 5 we present results from density-functional theory (DFT) calculations. There it can be seen that the calculated enthalpy of $AgMnO_4$-type $PbCrO_4$ becomes smaller than that of the stable monazite polymorph at 11.5 GPa. This supports the occurrence of the phase transition found in the experiments. The calculated transition pressure is about 3 GPa larger than the experimental pressure. Such differences are typical of DFT calculations.[25] The overestimation of the calculated transition pressure can be caused by the fact that calculations were performed at 0 K while experiments were carried out at 300 K,[25] but it could be also that nanosize effects reduce the transition pressure in experiments.[18] In order to determine which one is the possible dominant factor in this case, experiments as a function of temperature and particle size should be performed. The calculated crystal structure for

DOI: 10.1021/acs.jpclett.9b01978
J. Phys. Chem. Lett. 2019, 10, 4744−4751

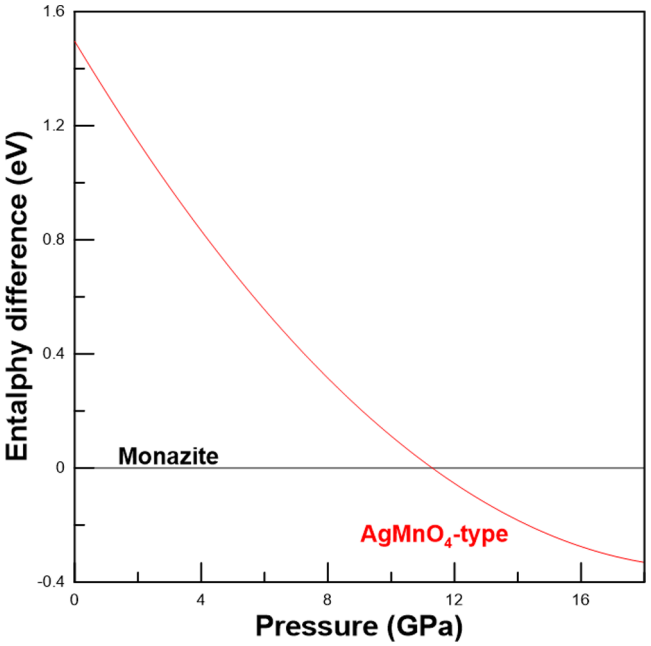

Figure 5. Enthalpy difference between monazite and $AgMnO_4$-type $PbCrO_4$ as a function of pressure taking monazite as reference.

$AgMnO_4$-type $PbCrO_4$ at 10.2 GPa is included in Table S2 of the Supporting Information. The agreement with the structure determined from experiments at 9.7 GPa is quite good.

By means of lattice-dynamics calculations we have computed the phonon frequencies of Raman- and infrared (IR)-active modes of $AgMnO_4$-type $PbCrO_4$. Factor group analysis indicates this polymorph has 36 Raman-active phonons ($\Gamma = 18A_g + 18B_g$) and 33 IR-active phonons ($\Gamma = 17A_u + 16B_u$). The calculated frequencies and pressure dependences of the different modes are summarized in Table S3 and S4 of the Supporting Information. The phonon distribution of Raman-active modes is very similar to the experimental phonon distribution. In the experiments only 20 modes are observed because several modes are nearly degenerated and because some modes have a weak Raman-scattering cross-section. In Table S3, it can be seen that experiments and calculations agree not only in phonon frequencies but also in their pressure dependences, which happen to be nonlinear. A remarkable fact is the presence of a soft mode (a B_g mode) with a frequency of 49.3 cm^{-1}, which indicates that the $AgMnO_4$-type polymorph is expected to become unstable at a pressure beyond those covered by the present study.[26] Regarding the IR-active modes, they have frequency distributions and pressure dependences similar to those of the Raman-active modes. The information given in Table S3 and S4 is fundamental to study the heat capacity and thermal expansion of the novel polymorph of $PbCrO_4$ as a function of pressure. Notice that both Raman- and IR-active phonons are distributed in three bands, with frequencies $\omega > 840$ cm^{-1}, 410 $cm^{-1} > \omega > 300$ cm^{-1}, and 240 $cm^{-1} > \omega$ (see Figure 4). The bands can be identified as internal stretching and bending modes of the CrO_4 tetrahedron and external modes that involve movements of Pb and CrO_4, respectively. The high-frequency stretching modes are the most intense modes as expected. As we comment above, the increase in the number of these modes after the phase transition is a fingerprint of the distortion of the CrO_4 tetrahedron induced by the transition.

From the XRD experiments we extracted the pressure dependence of the unit-cell parameters and volume of the two polymorphs. The results are shown in Figure 6 together with

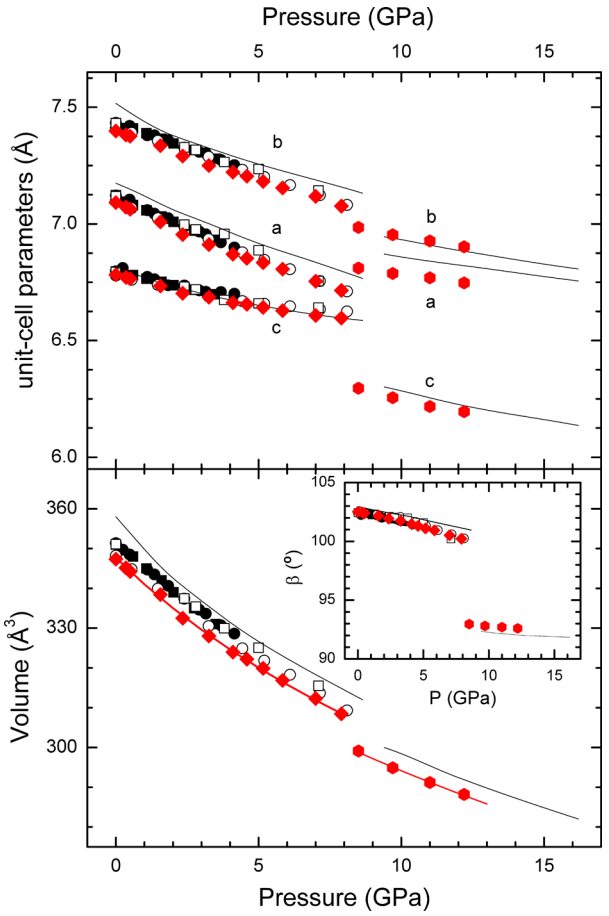

Figure 6. Pressure dependence of the unit-cell parameters and volume. The red symbols are the experimental results from this work. Black solid lines are the theoretical calculations. The red solid lines correspond to the third-order BM EOS fit. Black circles are results from ref 13, empty circles are from ref 12, and empty squares are from ref 10.

results from DFT calculations and results from the literature.[10,12,13] In the monazite structure, in spite of the small volume decrease of the nanorods, the pressure dependence is very similar to that of bulk $PbCrO_4$. The *a*-axis is the most compressible axis of monazite $PbCrO_4$ and the β angle gradually decreases under compression. The agreement with calculations is good not only for the low-pressure phase but also for the HP phase. After the phase transition, which involves a volume collapse (see Figure 6), the compression becomes nearly isotropic. In addition, the β angle is less affected by pressure in the HP polymorphs than in monazite. We have analyzed the pressure dependence of the volume of the two phases using a third-order Birch−Murnaghan equation of state (EOS).[27] The fit has been carried out using EOSFit.[28] For monazite-type $PbCrO_4$ nanorods the volume at ambient pressure (V_0), bulk modulus (B_0), and its pressure derivative (B_0') are $V_0 = 347.2(3)$ Å^3, $B_0 = 52.7(6)$ GPa, and $B_0' = 3.8(5)$, being the implied value[29] for the second pressure derivative $B_0'' = -0.0708$ GPa^{-1}. These values agree within uncertainties with the results obtained from bulk $PbCrO_4$, suggesting that the compressibility is not affected by the

DOI: 10.1021/acs.jpclett.9b01978
J. Phys. Chem. Lett. 2019, 10, 4744−4751

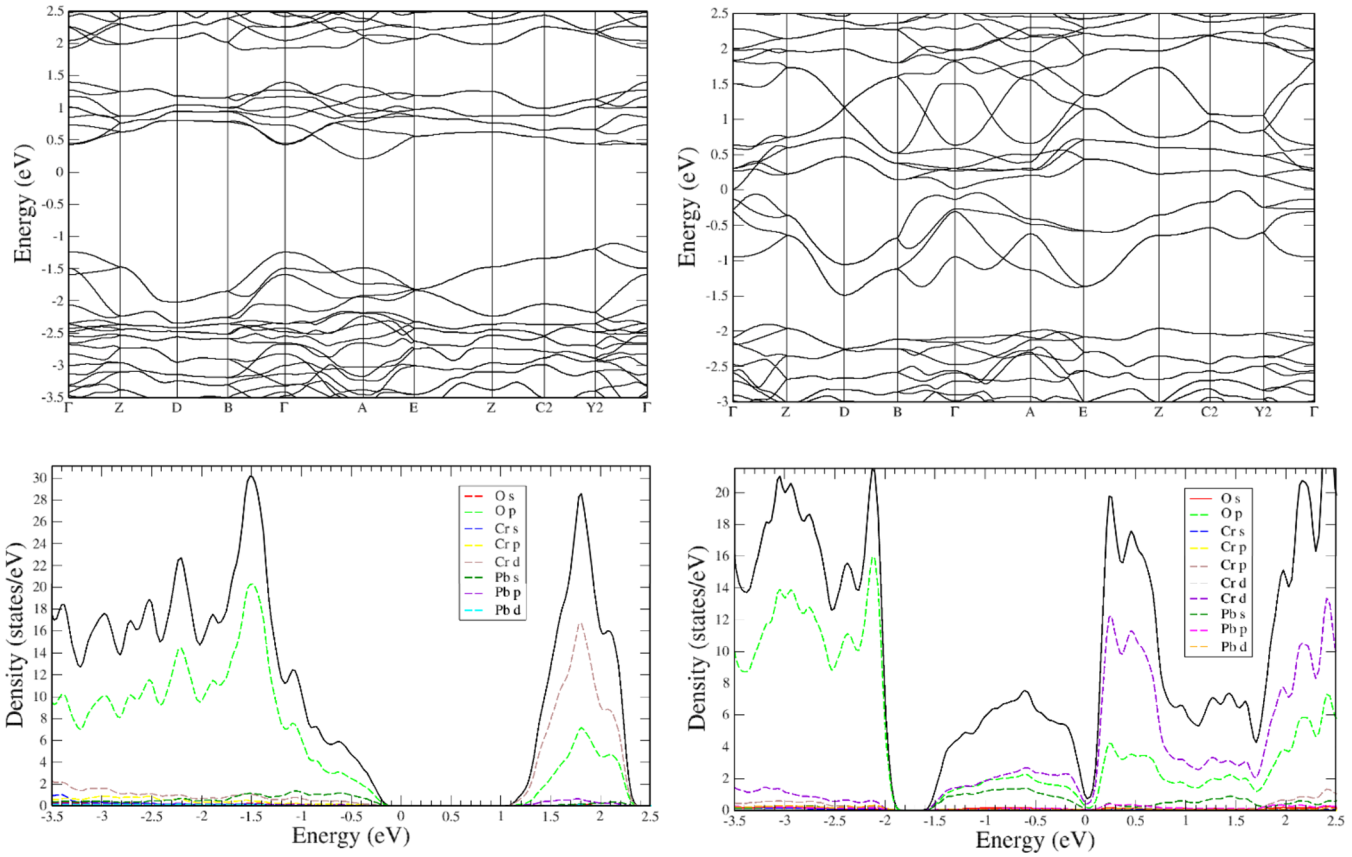

Figure 7. (Top) Band structure of $AgMnO_4$-type $PbCrO_4$ at 12.9 (left) and 44.2 GPa (right). (Bottom) Total and partial electronic density of state at 12.9 (left) and 44.2 GPa (right).

particle size. For the HP $AgMnO_4$-type phase we obtained V_0 = 334(2) Å^3, B_0 = 61(3) GPa, B_0' = 4.1(3), and B_0'' = −0.0656 GPa^{-1}. This indicates that the HP phase is less compressible than the low-pressure phase, which is consistent with the volume collapse associated with the transition, which shortens Pb−O, increasing their strength.

In order to analyze the anisotropy of the two phases observed in our study, we have determined for the first time the magnitudes and the directions of the principal axes of the compressibility tensor using PASCal.[30] The obtained results are given in Table S5 of the Supporting Information. There it can be seen that monazite $PbCrO_4$ is highly anisotropic, the largest compressibility being 7.3(1) × 10^{-3} GPa^{-1} and the smallest 1.2(1) × 10^{-3} GPa^{-1}. The directions of the most and least compressible axes are in the plane perpendicular to the unique *b*-axis. The first one makes a 66.4° angle with the *c*-axis and the second one makes a 150.9° with the same axis. In the HP phase the differences between the principal compressibilities are much smaller than in monazite, ranging them from 2.1(1) × 10^{-3} to 3.2(1) × 10^{-3} GPa^{-1}. In the HP phase, the most compressible axis makes a 15.2° angle with the *c* axis and the less compressible axis makes a −69.8° angle with it.

Pressure-induced metallization of oxides is a subject that has caught a lot of attention.[31] In particular, it has been proposed that in oxides like $PbCrO_4$ metallization could take place at relative low pressure due to the occurrence of a band gap collapse.[32] However, resistivity measurements have shown that bulk $PbCrO_4$ remains as a semiconductor material at least up to 35 GPa.[11] In the case of $PbCrO_4$ nanorods, we have observed a darkening of the sample at the phase transition, which might be a hint that metallization could take place under further compression.[33]

In order to explore the possible metallization of $AgMnO_4$-type $PbCrO_4$, we have carried out band-structure calculations. The calculated band structure and electronic density of states at two different pressures are shown in Figure 7. We found that this polymorph is an indirect band gap semiconductor with a small band gap of 1.31 eV at 12.9 GPa, which is consistent with the darkening of the sample. The maximum of the valence band is in the point of the Brillouin zone between Γ and Y2. The minimum of the conduction band is at the A point of the Brillouin zone. The bottom of the conduction band is dominated by Cr 3d and O 2p states and the top of the valence band by O 2p states (see Figure 7). Under compression, the band gap further red shifts with a pressure coefficient −32.7 meV/GPa. However, we found that not only the band gap closes but also there is a change in the topology of the band structure with several maxima developing in the valence band and the minimum of the conduction band moving to the Γ point. Our calculations indicate that the band gap reaches a critical value of 0 eV (onset of metallization) at 44.2 GPa, a low-pressure for a material with a band gap of 2.3 eV at ambient conditions.[11] As can be seen in Figure 7, at this pressure, the absolute maximum of the valence band is at a point between C2 and Y2 and the minimum of the conduction band is at the Γ point. According to the electronic density of states Pb, 6s states play a key role in metallization. This happens because of the increase of the contribution of Pb 6s states to the bottom of the conduction band in part due to the hybridizations between O 2p and Pb 6s orbitals triggered by

DOI: 10.1021/acs.jpclett.9b01978
J. Phys. Chem. Lett. 2019, 10, 4744−4751

compression.[34] In conclusion, our calculations suggest that $AgMnO_4$-type $PbCrO_4$ is a good candidate for pressure-driven metallization at pressures accessible to nowadays resistivity measurements in diamond-anvil cells.[35,36]

In summary, we have discovered a new polymorph of $PbCrO_4$, which is obtained in nanorods under a compression of 8.5 GPa. The novel HP phase has a monoclinic $AgMnO_4$-type structure, which was determined by means of XRD. The transition from the low-pressure phase into the HP phase is confirmed by Raman spectroscopy. DFT simulations confirm the reliability of the experimental findings and provide detailed information on the lattice vibrations. The compressibility has been analyzed for the two polymorphs determining not only the P−V EOS but also the magnitudes and directions of the principal axes of the compressibility tensor. Finally, our computational study shows that the HP polymorph has a narrow band gap energy (1.3 eV) and that pressure is expected to produce the metallization of $PbCrO_4$ nanorods at 44.2 GPa, a pressure accessible with state-of-the-art techniques. The present work therefore opens a new and promising avenue for the exploration of pressure-induced metallization in complex oxides, which at ambient conditions have a band gap in the visible (2.3 eV).

METHODS

Preparation of $PbCrO_4$ Rodlike Submicron Crystals. $PbCrO_4$ samples were prepared by a hydrothermal method according to the reported procedure.[37] Analytical grade chemicals of $Pb(CH_3COO)_2$, $K_2Cr_2O_7$, and the surfactants of polyvinylpyrrolidone (PVP, average MW, 1 300 000) were used without further purification. In a typical procedure, 1 mmol of $K_2Cr_2O_7$, 2 mol of $Pb(CH_3COO)_2$, 1 wt % PVP, and distilled water were mixed with vigorous stirring. The pH value of the mixture was adjusted to 7 by the addition of a 3 M NaOH solution. The final volume of the mixture was kept as 35 mL. After stirring for 10 min, the mixture was transferred into a Teflon-lined stainless-steel autoclave with a capacity of 50 mL for hydrothermal treatment at 140 °C for 20 h. The as-prepared product was separated by centrifugation and washed with H_2O twice, followed by drying at 60 °C in air overnight.

$PbCrO_4$ Nanorod Characterization. Scanning electron microscopy images were recorded with a JEOL JEM-6700F device. EDX measurements were carried out with the same system.

High-Pressure Generation. High-pressure experiments were performed using a Mao-type diamond-anvil cell with the diamond-culet size of 400 μm. $PbCrO_4$ samples were placed in a 200 μm diameter hole of a T301 steel gasket, which was preindented to a thickness of ∼50 μm. The loading was carefully done to avoid sample bridging between anvils.[38] Pressure was determined using a ruby-fluorescence method.[39] A 4:1 mixture of methanol and ethanol was used as the pressure transmitting medium for both XRD and Raman experiments.

X-ray Diffraction Measurements. HP angle-dispersive XRD experiments with a wavelength of 0.6199 Å and a focused beam size of about 4 × 7 μm^2 were performed at beamline 15U1, of Shanghai Synchrotron Radiation Facility (SSRF), China. XRD patterns were collected for 20−40 s at each pressure using a Mar-165 CCD detector and then were integrated with FIT2D.

Raman Spectroscopy. HP Raman spectra were recorded using a micro-Raman system assembled around a spectrometer (Acton SP2500, Princeton Instruments) and a liquid-nitrogen-cooled CCD (PyLoN:100B, Princeton Instruments). A 532 nm single-mode laser with power of 0.5 mW was utilized to excite the sample. The resolution of the Raman system was better than 1 cm^{-1}.

Overview of the Calculations. Density-functional theory simulations[40] were performed with the Vienna Ab-initio Simulation Package[41] employing projected-augmented wave pseudopotentials[42] and the generalized-gradient approximation. We have used AM05[43] functionals to describe the exchange correlation energy, which have been found to be the most accurate describing $PbCrO_4$, a cutoff energy of 520 eV, and a 3 × 3 × 3 Monkhorst−Pack[44] special *k*-points grid. The direct force-constant method was employed to calculate phonon frequencies.[45]

ASSOCIATED CONTENT

Supporting Information

The Supporting Information is available free of charge on the ACS Publications website at DOI: 10.1021/acs.jpclett.9b01978.

Tables with crystal structure data, Raman and IR modes (and pressure coefficients), and band structure, and electronic density of states of $AgMnO_4$-type $PbCrO_4$; compressibility tensor of the two polymorphs (PDF)

AUTHOR INFORMATION

Corresponding Author

*E-mail: daniel.errandonea@uv.es.

ORCID

Placida Rodriguez-Hernandez: 0000-0002-4148-6516

Alfonso Muñoz: 0000-0003-3347-6518

Daniel Errandonea: 0000-0003-0189-4221

Author Contributions

The manuscript was written through contributions of all authors. All authors have given approval to the final version of the manuscript.

Notes

The authors declare no competing financial interest.

ACKNOWLEDGMENTS

The authors acknowledge the financial support from the Spanish Ministerio de Ciencia, Innovación y Universidades, the Spanish Research Agency (AEI), the Generalitat Valenciana, and the European Fund for Regional Development (ERDF, FEDER) under Grants No. MAT2016-75586-C4-1/3-P and Prometeo/2018/123 (EFIMAT). Angle-dispersive XRD measurement was performed at the beamline 15U1 at the Shanghai Synchrotron Radiation Facility (SSRF).

REFERENCES

(1) Errandonea, D.; Muñoz, A.; Rodríguez-Hernández, P.; Proctor, J. E.; Sapiña, F.; Bettinelli, M. Theoretical and Experimental Study of the Crystal Structures, Lattice Vibrations, and Band Structures of Monazite-type $PbCrO_4$, $PbSeO_4$, $SrCrO_4$, and $SrSeO_4$. *Inorg. Chem.* **2015**, *54*, 7524−7535.

(2) Devi, S.; Prakash, S. G. Photoconductivity Studies of ($PbCrO_4$-HgO-ZnO) Composites. *Pramana* **1994**, *43*, 245−253.

(3) Cho, S. K.; Akbar, R.; Kang, J.; Lee, W. H.; Park, H. S. Electrodeposited Single-crystalline $PbCrO_4$ Microrods for Photoelectrochemical Water Oxidation: Enhancement of Minority Carrier Diffusion. *J. Mater. Chem. A* **2018**, *6*, 13312−13320.

DOI: 10.1021/acs.jpclett.9b01978
J. Phys. Chem. Lett. 2019, 10, 4744−4751

(4) Miseki, Y.; Kitao, O.; Sayama, K. Photocatalytic Water Oxidation over $PbCrO_4$ with 2.3 eV Band Gap in IO_3^-/I^- Redox Mediator under Visible Light. *RSC Adv.* **2015**, *5*, 1452−1455.
(5) Zhang, G. Q.; Liu, G.; Xu, Y.; Yang, J.; Li, Y.; Sun, X.; Chen, W.; Su, C. L. $PbCrO_4$ Yellow-pigment Nanorods: An Efficient and Stable Visible-light-active Photocatalyst for O_2 Evolution and Photodegradation. *Science China Materials* **2018**, *61*, 1033−1039.
(6) Amat, A.; Miliani, C.; Fantacci, S. Structural and Electronic Properties of the $PbCrO_4$ Chrome Yellow Pigment and of its Light Sensitive Sulfate-substituted Compounds. *RSC Adv.* **2016**, *6*, 36336−36344.
(7) Steger, S.; Oesterle, D.; Bretz, S.; Frenzel, L.; Stege, H.; Winkelmeyer, I.; Hahn, O.; Geiger, G. Kandinsky's Fragile Art. *Heritage Sci.* **2019**, *7*, 27.
(8) Clavier, N.; Podor, R.; Dacheux, N. Crystal Chemistry of the Monazite Structure. *J. Eur. Ceram. Soc.* **2011**, *31*, 941−976.
(9) Lee, H. C.; Cho, S. Ki.; Park, H. S.; Nam, K. M.; Bard, A. J. Visible Light Photoelectrochemical Properties of $PbCrO_4$, Pb_2CrO_5, and Pb_5CrO_8. *J. Phys. Chem. C* **2017**, *121*, 17561−17568.
(10) Bandiello, E.; Errandonea, D.; Martinez-Garcia, D.; Santamaria-Perez, D.; Manjon, F. J. Effects of High-pressure on the Structural, Vibrational, and Electronic Properties of Monazite-type $PbCrO_4$. *Phys. Rev. B: Condens. Matter Mater. Phys.* **2012**, *85*, No. 024108.
(11) Errandonea, D.; Bandiello, E.; Segura, A.; Hamlin, J. J.; Maple, M. B.; Rodriguez-Hernandez, P.; Muñoz, A. Tuning the Band Gap of $PbCrO_4$ Through High-pressure: Evidence of Wide-to-narrow Semiconductor Transitions. *J. Alloys Compd.* **2014**, *587*, 14−20.
(12) Errandonea, D.; Kumar, R. S. High-pressure Structural Transformations of $PbCrO_4$ up to 51.2 GPa: An Angle-dispersive Synchrotron X-ray Diffraction Study. *Mater. Res. Bull.* **2014**, *60*, 206−211.
(13) Gonzalez-Platas, J.; Muñoz, A.; Rodriguez-Hernandez, P.; Errandonea, D. High-pressure Single-crystal X-ray Diffraction of Lead Chromate: Structural Determination and Reinterpretation of Electronic and Vibrational Properties. *Inorg. Chem.* **2019**, *58*, 5966−5979.
(14) Knight, K. S. A Neutron Powder Diffraction Determination of the Thermal Expansion Tensor of Crocoite ($PbCrO_4$) Between 60 and 290 K. *Mineral. Mag.* **1996**, *60*, 963−972.
(15) Knight, K. S. A High Temperature Structural Phase Transition in Crocoite ($PbCrO_4$) at 1068 K: Crystal Structure Refinement at 1073 K and Thermal Expansion Tensor *Mineral. Mineral. Mag.* **2000**, *64*, 291−300.
(16) Zhang, J.; Lang, P. R.; Meyer, M.; Dhont, J. K. G. Synthesis and Self-assembly of Square Like $PbCrO_4$ Nanoplatelets Via Micelle-mediated Depletion Attraction. *Langmuir* **2013**, *29*, 4679−4687.
(17) Zhiani, R.; Es-haghi, A.; Sadeghzadeh, S. M.; Shamsa, F. Green Synthesis of $PbCrO_4$ Nnostructures Using Gum of Ferula Assa-foetida for Enhancement of Visible-light Photocatalytic Activity. *RSC Adv.* **2018**, *8*, 40934−40940.
(18) San Miguel, A. Nanomaterials under High-pressure. *Chem. Soc. Rev.* **2006**, *35*, 876−889.
(19) Johnston, M. B.; Herz, L. M. Hybrid Perovskites for Photovoltaics: Charge-Carrier Recombination, Diffusion, and Radiative Efficiencies. *Acc. Chem. Res.* **2016**, *49*, 146−154.
(20) Popescu, C.; Sans, J. A.; Errandonea, D.; Segura, A.; Villanueva, R.; Sapiña, F. Compressibility and Structural Stability of Nanocrystalline TiO_2 Anatase Synthesized from Freeze-Dried Precursors. *Inorg. Chem.* **2014**, *53*, 11598−11603.
(21) Crichton, W. A.; Parise, J. B.; Antao, S. M.; Grzechnik, A. Evidence for Monazite-, Barite-, and $AgMnO_4$ (distorted Barite)-type Structures of $CaSO_4$ at High Pressure and Temperature. *Am. Mineral.* **2005**, *90*, 22−27.
(22) Gleissner, J.; Errandonea, D.; Segura, A.; Pellicer-Porres, J.; Hakeem, M. A.; Proctor, J. E.; Raju, S. V.; Kumar, R. S.; Rodrıguez-Hernandez, P.; Muñoz, A.; Lopez-Moreno, S.; Bettinelli, M. Monazite-type $SrCrO_4$ under compression. *Phys. Rev. B: Condens. Matter Mater. Phys.* **2016**, *94*, 134108.
(23) Errandonea, D. High-pressure Phase Transitions and Properties of MTO_4 Compounds with the Monazite-type Structure. *Phys. Status Solidi B* **2017**, *254*, 1700016.
(24) Hakeem, M. A.; Jackson, D. E.; Hamlin, J. J.; Errandonea, D.; Proctor, J. E.; Bettinelli, M. High Pressure Raman, Optical Absorption, and Resistivity Study of $SrCrO_4$. *Inorg. Chem.* **2018**, *57*, 7550−7557.
(25) López-Moreno, S.; Errandonea, D.; Pellicer-Porres, J.; Martínez-García, D.; Patwe, S. J.; Achary, S. N.; Tyagi, A. K.; Rodríguez-Hernández, P.; Muñoz, A.; Popescu, C. Stability of $FeVO_4$ under Pressure: An X-ray Diffraction and First-Principles Study. *Inorg. Chem.* **2018**, *57*, 7860−7876.
(26) Errandonea, D.; Pellicer-Porres, J.; Martınez-Garcıa, D.; Ruiz-Fuertes, J.; Friedrich, A.; Morgenroth, W.; Popescu, C.; Rodrıguez-Hernandez, P.; Muñoz, A.; Bettinelli, M. Phase Stability of Lanthanum Orthovanadate at High Pressure. *J. Phys. Chem. C* **2016**, *120*, 13749−13762.
(27) Birch, F. Finite Elastic Strain of Cubic Crystals. *Phys. Rev.* **1947**, *71*, 809−824.
(28) Angel, R. J.; Alvaro, M.; Gonzalez-Platas, J. EosFit7c a Fortran Module (library) for Equation of State Calculations. *Z. Kristallogr. - Cryst. Mater.* **2014**, *229*, 405−419.
(29) Errandonea, D.; Ferrer-Roca, Ch.; Martínez-Garcia, D.; Segura, A.; Gomis, O.; Muñoz, A.; Rodríguez-Hernández, P.; López-Solano, J.; Alconchel, S.; Sapiña, F. High-pressure X-ray Diffraction and Ab Initio Study of Ni_2Mo_3N, Pd_2Mo_3N, Pt_2Mo_3N, Co_3Mo_3N, and Fe_3Mo_3N: Two Families of Ultra-incompressible Bimetallic Interstitial Nitrides. *Phys. Rev. B: Condens. Matter Mater. Phys.* **2010**, *82*, 174105.
(30) Cliffe, M. J.; Goodwin, A. L. PASCal: A Principal Axis Strain Calculator for Thermal Expansion and Compressibility Determination. *J. Appl. Crystallogr.* **2012**, *45*, 1321−1329.
(31) Bai, L.; Li, Q.; Corr, S. A.; Meng, Y.; Park, C.; Sinogeikin, S. V.; Ko, C.; Wu, J.; Shen, G. Pressure-induced Phase Transitions and Metallization in VO_2. *Phys. Rev. B: Condens. Matter Mater. Phys.* **2015**, *91*, 104110.
(32) Errandonea, D.; Garg, A. B. Recent Progress on the Characterization of the High-pressure Behaviour of AVO_4 Orthovanadates. *Prog. Mater. Sci.* **2018**, *97*, 123−169.
(33) Barreda-Argüeso, J. A.; Nataf, L.; Aguado, F.; Hernández, I.; González, J.; Otero de la Roza, A.; Luaña, V.; Jia, Y.; Jin, C.; Kim, B.; Kim, K.; Min, B. I.; Heribert, W.; Jephcoat, A. P.; Rodríguez, F. Pressure-induced Spin Transition and Site-selective Metallization in $CoCl_2$. *Sci. Rep.* **2019**, *9*, 5448.
(34) Monteseguro, V.; Ruiz-Fuertes, J.; Contreras-Garcia, J.; Rodriguez-Hernandez, P.; Muñoz, A.; Errandonea, D. Unveiling the Origin of the Bandgap of $PbMoO_4$ under High Pressure. *Appl. Phys. Lett.* **2019**, *115*, No. 012102.
(35) Yang, L.; Dai, L.; Li, H.; Hu, H.; Liu, K.; Pu, C.; Hong, M.; Liuc, P. Pressure-induced Metallization in $MoSe_2$ under Different Pressure Conditions. *RSC Adv.* **2019**, *9*, 5794−5803.
(36) Hu, T.; Cui, X.; Wang, J.; Zhong, X.; Chen, Y.; Zhang, J.; Li, X.; Yang, J.; Gao, C. The Electrical Properties of Tb-Doped CaF2 Nanoparticles under High Pressure. *Crystals* **2018**, *8*, 98.
(37) Liang, J.; Peng, Q.; Wang, X.; Zheng, X.; Wang, R.; Qiu, X.; Nan, C.; Li, Y. Chromate Nanorods/nanobelts: General Synthesis, Characterization, and Properties. *Inorg. Chem.* **2005**, *44*, 9405−9415.
(38) Errandonea, D.; Muñoz, A.; Gonzalez-Platas, J. Comment on "High-pressure X-ray Diffraction Study of YBO_3/Eu^{3+}, $GdBO_3$, and $EuBO_3$: Pressure-induced Amorphization in $GdBO_3$. *J. Appl. Phys.* **2014**, *115*, 216101.
(39) Mao, H. K.; Xu, J.; Bell, P. M. Calibration of the Ruby Pressure Gauge to 800 kbar under Quasi-hydrostatic Conditions. *J. Geophys. Res.* **1986**, *91*, 4673−4676.
(40) Hohenberg, P.; Kohn, W. Inhomogeneous Electron Gas. *Phys. Rev.* **1964**, *136*, B864−B871.
(41) Kresse, G.; Furthmüller, J. Efficient Iterative Schemes for Ab Initio Total-energy Calculations Using a Plane-wave Basis Set. *Phys. Rev. B: Condens. Matter Mater. Phys.* **1996**, *54*, 11169−11186.

DOI: 10.1021/acs.jpclett.9b01978
J. Phys. Chem. Lett. 2019, 10, 4744−4751

(42) Blöchl, P. E. Projector Augmented-wave Method. *Phys. Rev. B: Condens. Matter Mater. Phys.* **1994**, *50*, 17953−17979.
(43) Mattsson, A. E.; Armiento, R.; Paier, R. J.; Kresse, G.; Wills, J. M.; Mattsson, T. R. The AM05 Density Functional Applied to Solids. *J. Chem. Phys.* **2008**, *128*, No. 084714.
(44) Monkhorst, H. J.; Pack, J. D. Special Points for Brillouin-zone Integrations. *Phys. Rev. B* **1976**, *13*, 5188−5192.
(45) Parlinski, K.; Li, Z. Q.; Kawazoe, Y. First-principle Determination of the Soft Mode in Cubic ZrO_2. *Phys. Rev. Lett.* **1997**, *78*, 4063−4066.

DOI: 10.1021/acs.jpclett.9b01978
J. Phys. Chem. Lett. 2019, 10, 4744−4751